

Text Rationalization for Robust Causal Effect Estimation

Lijinghua Zhang* Hengrui Cai*

Abstract

Recent advances in natural language processing have enabled the increasing use of text data in causal inference, particularly for adjusting confounding factors in treatment effect estimation. Although high-dimensional text can encode rich contextual information, it also poses unique challenges for causal identification and estimation. In particular, the positivity assumption, which requires sufficient treatment overlap across confounder values, is often violated at the observational level, when massive text is represented in feature spaces. Redundant or spurious textual features inflate dimensionality, producing extreme propensity scores, unstable weights, and inflated variance in effect estimates. We address these challenges with Confounding-Aware Token Rationalization (CATR), a framework that selects a sparse necessary subset of tokens using a residual-independence diagnostic designed to preserve confounding information sufficient for unconfoundedness. By discarding irrelevant texts while retaining key signals, CATR mitigates observational-level positivity violations and stabilizes downstream causal effect estimators. Experiments on synthetic data and a real-world study using the MIMIC-III database demonstrate that CATR yields more accurate, stable, and interpretable causal effect estimates than existing baselines.

1 Introduction

Causal inference aims to uncover cause-and-effect relationships from observational data and plays a central role in scientific decision-making across the social, biomedical, and computational sciences (Rubin, 1974; Holland, 1986; Pearl, 2000). A primary objective in causal inference is to estimate treatment effects, such as the average treatment effect (ATE), the expected difference in outcomes between treated and untreated groups, from observational data (Imbens and Rubin, 2015). Identification of these estimands requires the assumptions of consistency, unconfoundedness, and positivity (Pearl, 2000). To satisfy *unconfoundedness*—the absence of unmeasured confounding—it is common practice to include as much relevant information as possible. While traditional analyses rely on structured

*Department of Statistics, University of California, Irvine. Emails: lijinghz@uci.edu, hengrc1@uci.edu

covariates, recent advances in natural language processing (NLP; e.g., [Devlin et al., 2019](#); [Roumeliotis and Tselikas, 2023](#); [Touvron et al., 2023](#); [Yang et al., 2025](#)) have enabled the systematic use of *unstructured text* in causal inference. High-dimensional text, such as clinical notes, legal documents, and free-form narratives, often encodes latent contextual and massive information that simultaneously influence treatment assignment and outcome ([Wei et al., 2022](#); [Zhao et al., 2023](#)). As a result, incorporating text has become a promising strategy for confounding adjustment, with the potential to strengthen unconfoundedness by surfacing otherwise unrecorded confounders ([Egami et al., 2022](#); [Feder et al., 2022](#)).

A motivating example arises in critical care, where researchers seek to estimate the effect of intravenous fluid therapy for patients at risk of sepsis in intensive care units (ICUs). Randomized trials for such interventions are seldom feasible in emergency settings, so retrospective analyses rely on observational data. The Medical Information Mart for Intensive Care III (MIMIC-III) database ([Johnson et al., 2016](#)) provides a rich resource for this purpose, combining structured electronic health record variables (e.g., demographics, vital signs, laboratory measurements) with unstructured clinical notes (e.g., nursing progress notes, physician admission summaries). As illustrated in Table 1, these clinical notes capture rich contextual information about disease severity, comorbidities, and clinician assessments, which are not encoded in tabular or structured electronic health records yet may plausibly confound both treatment assignment and outcomes. This example shows that *unstructured text may encode essential confounding signals* which, if ignored, can lead to biased causal effect estimates.

Despite this promise, incorporating unstructured text poses unique challenges for causal effect identification, particularly for the *positivity* assumption. Positivity requires that every unit has a propensity score (defined as the probability of receiving treatment given their confounders) bounded away from 0 and 1, indicating sufficient treatment overlap across all confounder combinations. Yet, this assumption is particularly vulnerable in text-based causal inference. Two key mechanisms contribute to this deterioration: (i) text often contains *irrelevant or spurious features* that act as redundant proxies, inflating dimensionality without contributing meaningful confounding information and thereby obscuring the true confounding patterns; and (ii) the *high-dimensional, sparse, and discrete* nature of text substantially enlarges the covariate space, reducing overlap between treatment groups and making it difficult to extrapolate treatment assignment. This mismatch phenomenon between underlying and observed overlap leads to what we term **an observational-level positivity violation**: empirical overlap fails caused not by positivity in the data-generating process, but by the high-dimensional and redundant proxies that expand the covariate space. In practice, such violations induce extreme estimated propensity scores that concentrate near 0 or 1, yielding unstable inverse probability weighted (IPW) estimates, and inflated variance in doubly robust (DR) estimators ([Belloni et al., 2014](#); [Keller et al., 2015](#); [Feder et al., 2022](#)).

A controlled simulation illustrates this phenomenon. Treatment assignment depends on a single latent confounder C , and the positivity holds by design in the data-generating process. The observational data, however, consist of

Table 1: Example clinical note with color-coded highlights for information often missing from structured variables. **Gray**: information that is already captured by structured variables (e.g., vitals, labs, etc., with a complete list of structured variables provided in supplementary materials); **Yellow**: patient behavior and response to interventions, such as agitation, confusion, or non-cooperation; **Orange**: diagnostic uncertainty or preliminary clinical impressions; **green**: procedural context, such as the insertion of tubes or medical devices; **Blue**: social and familial context, including living arrangements and the involvement of family members in clinical decisions.

Pt is an 83YO male admitted to MICU for treatment of pleural effusion, ptx, pnx, hypoxia, hypotension.
ALL: NKDA
Please see FHPA for details of admission.
Review of Systems
NEURO: Pt is confused and inappropriate at times. He is capable of following commands but generally chooses not to. He becomes belligerent and agitated with any interventions, despite explanations.
RESP: Sats have been 92–94% on NRB; he refused to keep it on, and was changed over to 6L NC with sats remaining in low 90's. LS very diminished, especially LLL.
C-V: HR 80's, NSR, no ectopy. EKG in EW with ? new ST depressions in V3–V6. Denies CP. CK #1 4006 with negative MB fraction and slightly elevated Troponin. CK #2 pending. BP has been borderline, though pt apparently runs low. Currently, however, BP is in low 80's, and he is receiving a fluid bolus.
GI: Belly soft, NT, ND, active BS. No stool.
ID: Low-grade temp; cx's in EW. ? pnx on CXR. Got Ceftriaxone and Levoquin in EW.
HEME: PT/PTT extremely elevated this AM, but were drawn from Quinton cath (likely contaminated with heparin despite removing it from line).
RENAL: Last dialyzed [5-1]. Pt is anuric at baseline.
Access
LLA PIV, RSC Quinton catheter
Social
Pt's spokesperson is his [First Name9 (NamePattern2) 3961] [Doctor LN]; he states he lives with his grandson, and has 3 dtrs.
Assessment and Plan
A: borderline oxygenation and BP; pt has little tolerance for interventions.
P: follow VS, oxygenation, temps, assess for evidence of ischemia or infection; plan is for U/S-guided pleural tap; contact family to address code status.

high-dimensional, sparse proxy features X . Details of the experimental setup are provided in the supplementary material. As shown in Figure 1A, treated and control units overlap well in the underlying true confounder (C) space. Mapping the data into the proxy (X) space markedly reduces the overlap between treatment groups. To visualize the effect, we project the data onto the first two principal components and plot marginal kernel density estimates (KDEs), as shown in Figure 1B. Consequently, the estimated propensity scores $\hat{g}(X)$ concentrate more mass near 0 and 1 than the ground truth, frequently exceeding clipping thresholds of 0.03 and 0.97 in (Figure 1C), which induces heavy-tailed inverse probability weights and inflated the variance of IPW-based estimators for causal effects. Moreover, as the proxy dimension increases, the fraction of clipped samples rises (Figure 1D). This behavior mirrors empirical patterns in high-dimensional text confounders, where irrelevant tokens inflate dimensionality without improving confounding adjustment.

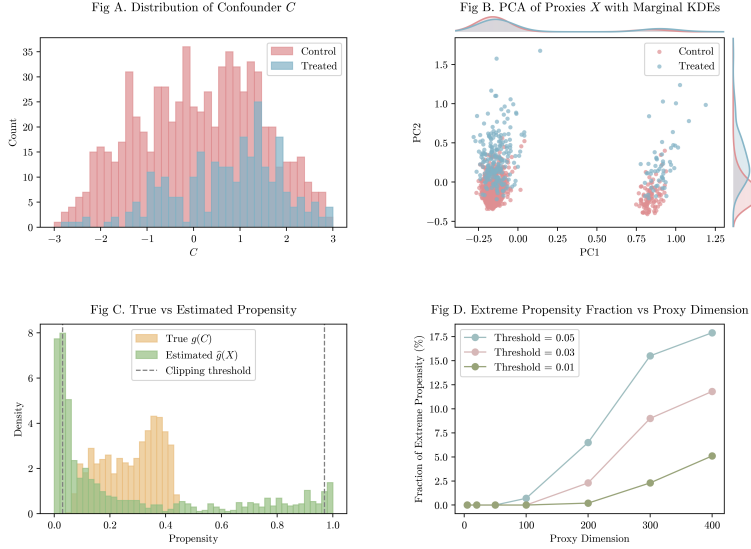


Figure 1: Illustration of the observational-level positivity violation induced by high-dimensional proxies. Fig A shows reasonable overlap of confounder between treated and control groups in the latent confounder space. Fig B shows stronger separation on some direction after mapping to high-dimensional sparse proxies X , as seen from projections onto the first two principal components with marginal KDEs. Fig C shows the estimated propensities concentrates more mass near the extremes (vertical dashed lines indicate clipping thresholds at 0.03 and 0.97), highlighting inflated variance in weighting. Fig D shows that as proxy dimension increases, the clipping fraction rises rapidly, demonstrating how redundant proxies dilute effective overlap and exacerbate observational-level positivity violations.

These challenges motivate our focus in this paper: *How can we extract a statistically sufficient, low-dimensional representation of text that preserves unconfoundedness while mitigating observational-level positivity violations?* Prior work suggests that unfiltered, high-dimensional text representations impair overlap and destabilize causal estimators. Addressing this issue requires moving beyond generic text encoders and loss functions toward methods that explicitly target the statistical properties necessary for valid causal inference.

1.1 Related Work

Building on the challenges identified above, we review existing approaches for estimating causal effects when high-dimensional and unstructured text serves as confounders. Broadly, current methods fall into three categories: (1) text-based representation learning for causal inference, (2) stabilizing propensity score estimation for structured data, and (3) token-level text rationalization for

interpretable subset selection.

Early work on **incorporating unstructured text for causal inference** reduced dimensionality through topic models (Roberts et al., 2020; Egami et al., 2022) or bag-of-words representations (Wood-Doughty et al., 2018). These methods provide coarse summaries that struggle to capture nuanced linguistic features. The advent of transformer-based language models, such as BERT (Devlin et al., 2019) and LLaMA (Touvron et al., 2023), marked a shift toward rich and context-aware text embeddings, which have become widely used across biomedical prediction tasks (Alsentzer et al., 2019; Huang et al., 2019; Lee et al., 2020). These representations have been paired with neural causal architectures originally developed for high-dimensional data, including TARNet/CFRNet (Shalit et al., 2017), and DragonNet (Shi et al., 2019). Subsequent work adapts these models more explicitly to the structure of text. One line focuses on representation learning: for example, CausalBERT (Veitch et al., 2020) augments language-modeling objectives while jointly predicting treatment and outcome. A second line employs latent-variable models, including CEVAE (Louizos et al., 2017), TEDVAE (Zhang et al., 2021), and DIVA (Zhou and He, 2023). These works infer latent confounders and decompose text into interpretable factors. While these methods reduce dimensionality, they do *not directly address the observational-level positivity violation* caused by redundant proxies in high-dimensional text. Moreover, latent factors can be *difficult to interpret and sensitive to model assumptions*.

Parallel developments in the statistical literature offers several strategies to **stabilize propensity score estimation for structured data** and limiting the influence of extreme weights. One class of methods operates directly on the propensity score distribution, including trimming or clipping observations near 0 or 1 (Crump et al., 2009; Lee et al., 2011) and rescaling inverse probability weighting to control variance inflation (Cole and Hernán, 2008; Li et al., 2018; van der Laan et al., 2025). Another class, covariate balancing methods (e.g., Imai and Ratkovic, 2014), enforces balance conditions directly during estimation to reduce reliance on extreme propensities. However, these techniques are *not well suited to high-dimensional text-based confounding*, where positivity violations arise at the observational level even when the positivity assumption holds in the underlying data-generating process. Post-hoc adjustments such as trimming or clipping discard valid samples without resolving token-level imbalance, and traditional balancing methods assume low-dimensional and interpretable covariates, whereas text embeddings are high-dimensional and lack explicit semantic axes along which balance can be imposed.

To address **the high dimensionality of text while providing interpretable subset selection**, selective rationalization methods aim to extract concise token subsets that preserve predictive performance (Bao et al., 2018; Jain et al., 2020; Guerreiro and Martins, 2021; Antognini and Faltings, 2021). Early approaches used non-differentiable selectors (Lei et al., 2016; Yu et al., 2019), whereas later work introduced differentiable relaxations such as the Gumbel-Softmax for end-to-end training (Bastings et al., 2019; Geng et al., 2020; Sha et al., 2021; Liu et al., 2022). Recent efforts (Cai et al., 2023; Zhang et al.,

2023) have connected rationalization to causal notions of necessity and sufficiency (Tian and Pearl, 2000), though predominantly in *predictive* rather than inference settings. Crucially, existing rationalization techniques do *not evaluate whether selected tokens preserve the confounding information required for valid causal identification*.

1.2 Contributions

To overcome the aforementioned challenges posed by high-dimensional text confounders in causal effect estimation, we propose selecting a sparse subset of tokens that is sufficient for confounding adjustment while mitigating observational-level positivity violations and improving interpretability. Our approach builds on a residual dependence measurement grounded in the Hilbert–Schmidt Independence Criterion (HSIC) (Gretton et al., 2007), a kernel-based measure widely used for independence testing and causal structure discovery (Zhang et al., 2011; Strobl et al., 2019). The key insight is that if a selected token subset preserves unconfoundedness, then the residuals of the treatment and outcome models should be independent; residual HSIC provides a falsification test for this sufficiency. Leveraging this connection, our method identifies subsets that retain essential confounding information, thereby mitigating observational-level positivity violations. Our **contributions** are fourfold.

Conceptually, to our knowledge, this is the first work on causal effect estimation with high-dimensional text that emphasizes interpretable text rationalization for robustness. We formalize how high-dimensional or text confounding can induce *observational-level positivity violations*. Through a controlled experiment (Figure 1), we show that redundant or spurious tokens can generate near-deterministic treatment assignment even when the underlying positivity is satisfied. This highlights the need for selecting token subsets that are necessary and sufficient for confounder adjustment.

Methodologically, we introduce *Confounding-Aware Token Rationalization (CATR)*, a new token-level rationalization framework developed specifically for causal identification with high-dimensional text. CATR selects sparse token subsets by minimizing a residual HSIC criterion under a sparsity penalty, ensuring that the retained tokens preserve the conditional independence structure required for unconfoundedness while simultaneously improving empirical overlap. Incorporating residual HSIC as a penalization term within a token-level rationalization framework is, to our knowledge, new to the literature. Unlike prior uses of HSIC for general independence testing or predictive feature selection, CATR explicitly targets causal sufficiency for causal adjustment, by minimizing residual treatment-to-outcome dependence. This yields a principled and computationally efficient approach for reducing redundant textual proxies, mitigating observational-level positivity violations, and stabilizing downstream causal estimators.

Theoretically, we establish conditions under which residual HSIC provides a valid falsification test for sufficiency of the selected token subset. Under the proposed CATR framework, we derive nonasymptotic error bounds for the neural

network estimators of the nuisance components and show that the corresponding augmented IPW estimator for ATE estimation achieves \sqrt{n} -consistency and asymptotic normality. These results position CATR within the semiparametric efficiency framework.

Empirically, through semi-synthetic experiments and a real-world analysis of the MIMIC-III sepsis cohort, we demonstrate that CATR consistently improves overlap, reduces weight instability and variance, and yields more stable and interpretable ATE estimates compared to existing text-based causal methods. These gains highlight the practical importance of token-level sufficiency for reliable causal inference with text.

The rest of the paper is organized as follows. Section 2 introduces the setup for the text-based causal effect estimation and formalizes the observational-level positivity violation. Section 3 establishes the role of HSIC as a criterion for subset causal sufficiency. Section 4 presents the proposed CATR framework, including the learning architecture, objective function, and an extension to multimodal data, with theoretical properties established in Section 5. Section 6 reports empirical results from both synthetic studies and a real-world analysis of the MIMIC-III sepsis cohort. Section 7 concludes our paper with future directions. The supplementary materials collect all proofs, additional implementation details, more details on synthetic data construction and the MIMIC-III application, and all codes to reproduce our experiments.

2 Notation and Problem Formulation

We study causal effect estimation in observational studies where confounding is embedded in unstructured text. Let (\mathbf{W}, T, Y) denote random variables for the text, treatment, and outcome, respectively. We observe n independent and identically distributed samples $\{(\mathbf{w}_i, t_i, y_i)\}_{i=1}^n$, where $\mathbf{w}_i = (w_{i1}, \dots, w_{iL_i})$ is the observed text for unit i of length L_i , $t_i \in \{0, 1\}$ is the binary treatment indicator, and $y_i \in \{0, 1\}$ (or \mathbb{R}) is the observed outcome. Let $\Lambda(\mathbf{W})$ as the embedding of \mathbf{W} produced by a pre-trained encoder $\Lambda(\bullet)$. Following the potential outcome framework (Rubin, 1974), each unit has two potential outcomes, $Y(0)$ and $Y(1)$, under control and treatment, respectively. Although the full text \mathbf{W} contains rich contextual information, only a subset $\mathbf{W}^c \subset \mathbf{W}$ encodes the true confounding signals that jointly affect both treatment T and outcome Y . The remaining tokens, denoted as \mathbf{W}^r , are irrelevant or redundant. Throughout, we adopt the causal structure illustrated in Figure 2, in which the causal pathways operate through \mathbf{W}^c but not through \mathbf{W}^r . We define the propensity score and the conditional mean outcome functions as $g(\mathbf{w}^c) = \Pr(T = 1 \mid \mathbf{W}^c = \mathbf{w}^c)$ and $Q_t(\mathbf{w}^c) = \mathbb{E}[Y \mid T = t, \mathbf{W}^c = \mathbf{w}^c]$, respectively, given the true confounding signals. And let $\hat{g}(\cdot)$ and $\hat{Q}_t(\cdot)$ denote their corresponding estimators, which may be constructed using either the full text \mathbf{W} or a selected subset.

Our target estimand is the average treatment effect (ATE) $\tau = \mathbb{E}\{Y(1) - Y(0)\}$. To validly identify τ from the observational data, we consider three identification assumptions, as standard requirements in causal inference literature (see,

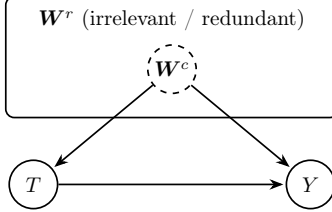


Figure 2: Causal diagram illustrating text-based confounding: \mathbf{W}^c (confounding tokens) affects both treatment T and outcome Y , while \mathbf{W}^r denotes irrelevant or redundant tokens.

e.g., [Imbens and Rubin, 2015](#); [Farrell et al., 2021](#); [Feder et al., 2022](#)), including unconfoundedness, positivity, and consistency. Specifically, given the observed text \mathbf{W} and its true confounding signals \mathbf{W}^c , to identify τ , identification requires:

Assumption (A1) (Unconfoundedness) The true confounding signals \mathbf{W}^c (contained within the observed text \mathbf{W}) are sufficient for adjustment:

$$\{Y(0), Y(1)\} \perp T \mid \mathbf{W}^c.$$

Assumption (A2) (Positivity on True Signals) Each unit has a nonzero probability of receiving both treatment and control conditional on the true confounding signals \mathbf{W}^c :

$$0 < p_1 \leq \Pr(T = 1 \mid \mathbf{W}^c) \leq p_2 < 1, \quad \forall \mathbf{W}^c.$$

Assumption (A3) (Consistency) The observed outcome corresponds to the potential outcome under the received treatment: $Y = Y(T)$.

While Assumptions (A1)–(A3) are typically imposed when working with structured covariates, their extension to text data introduces additional complexities ([Feder et al., 2022](#)). As discussed in Section 1, the unconfoundedness assumption (A1) is plausibly satisfied when rich text is included, because clinical or contextual narratives often record many factors influencing both treatment decisions and outcomes ([Wei et al., 2022](#); [Zhao et al., 2023](#)). In contrast, the positivity assumption, that every unit has a propensity score bounded away from 0 and 1, is particularly fragile when adjusting for text confounders. Since the true confounders \mathbf{W}^c are unknown, analysts often condition on the full set of tokens \mathbf{W} . This leads to high-dimensional covariates, unstable propensity score estimates, and diminished overlap between treatment groups, as illustrated in Table 1 and Figure 1.

We refer to this phenomenon as an **observational-level positivity violation**: although the true treatment mechanism $g(\mathbf{w}^c)$ remains well-balanced conditioned on the true confounding signals \mathbf{w}^c , the empirical estimates $\hat{g}(\mathbf{w})$ concentrate more mass near 0 and 1 because redundant or irrelevant tokens distort the high-dimensional covariate space. As a result, effective overlap is lost even though Assumption (A2) holds. Formally, we have:

Definition 2.1 (Observational-level positivity violation). Let $g(\mathbf{w}) = \Pr(T = 1 \mid \mathbf{W} = \mathbf{w})$ denote the population-level treatment mechanism, and $\hat{g}(\mathbf{w}) = \Pr_n(T = 1 \mid \mathbf{W} = \mathbf{w})$ its empirical estimate. An *observational-level positivity violation* occurs when there exists $\mathbf{w} \in \text{supp}(\mathbf{W})$ such that $\hat{g}(\mathbf{w}) \notin [\epsilon, 1 - \epsilon]$ for some $0 < \epsilon < 1$, even though the true treatment assignment mechanism satisfies $g(\mathbf{w}^c) \in [\epsilon, 1 - \epsilon]$ given the true confounding subset \mathbf{w}^c . Equivalently, at the empirical level, for some tolerance $\delta > 0$, we have

$$\mathbb{P}_n\{\hat{g}(\mathbf{W}) \notin [\epsilon, 1 - \epsilon]\} \geq \delta.$$

Importantly, this notion differs from the positivity violation at true data generating process, which lead to non-identifiable causal effects (Pearl, 2000; Imbens and Rubin, 2015; Feder et al., 2022). Observational-level violations, instead, preserve identifiability but complicate estimation by inflating variance and degrading overlap.

To mitigate this violation, **our goal** to learn a sparse text selector

$$S(\cdot) : \mathbf{w}_i \longrightarrow \tilde{\mathbf{w}}_i = S(\mathbf{w}_i),$$

which maps each observed text sequence \mathbf{w}_i to a shorter subsequence $\tilde{\mathbf{w}}_i$ of length $d_i \ll L_i$, such that $\tilde{\mathbf{w}}_i$ approximates the true confounding component \mathbf{w}_i^c . To ensure interpretability and statistical stability, the selector is subject to a sparsity constraint, such as a token budget or an entropy-based regularization that encourages compact subsequences. If successful, standard identification assumptions hold when conditioning on $\tilde{\mathbf{W}}$ as well as \mathbf{W}^c , namely:

$$\underbrace{(Y(0), Y(1)) \perp T \mid \tilde{\mathbf{W}}}_{\text{Unconfoundedness}}, \quad \underbrace{\epsilon \leq g(\tilde{\mathbf{W}}) \leq 1 - \epsilon}_{\text{Positivity}}, \quad \underbrace{Y = Y(T)}_{\text{Consistency}}.$$

The first condition ensures that the selected subsequence retains all confounding information from the original text, the second enforces overlap between treatment groups by bounding the propensity score away from 0 and 1, and the last links the observed outcome to the potential outcome under the received treatment, holding whenever treatment is well-defined and regardless of the selection choice.

3 HSIC Measurement for Subset Sufficiency

The goal of the sparse text selector is to remove irrelevant or redundant tokens to improve covariate overlap. However, aggressive filtering risks discarding text features that jointly affect treatment and outcome, thereby violating unconfoundedness. To guard against this, we consider a penalty based on the Hilbert–Schmidt Independence Criterion (HSIC) (Gretton et al., 2007), which measures statistical dependence through kernel embeddings. The key idea is that, after conditioning on a sufficient selected text subset, the residuals of the treatment and outcome models should be independent. HSIC provides an efficient, fully nonparametric diagnostic for assessing this residual dependence during rationalization.

Specifically, given two random variables U and V , let k_U and k_V be characteristic kernels with corresponding Gram matrices $K, L \in \mathbb{R}^{n \times n}$ over n samples. Define $H = I_n - (1/n)\mathbf{1}_n\mathbf{1}_n^\top$, where I_n is the $n \times n$ identity matrix and $\mathbf{1}_n$ is an n -dimensional vector of ones. Then the empirical HSIC is given by

$$\widehat{\text{HSIC}}(U, V) = \frac{1}{(n-1)^2} \text{tr}(KHLH),$$

where $\text{tr}(\cdot)$ denotes the matrix trace. HSIC is always nonnegative and equals zero if and only if U and V are independent when characteristic kernels. This makes HSIC a natural tool for detecting whether a selected subset of tokens preserves the confounding information encoded in the full text. To establish the diagnostic role of HSIC for subset sufficiency, i.e., detecting whether a selected token subset $\tilde{\mathbf{W}}$ preserves the true confounding signals \mathbf{W}^c , we adopt a standard additive-noise structural model widely used in causal discovery and nonparametric identification (Hoyer et al., 2009; Peters et al., 2014, 2017).

Assumption (A4) (Additive independent noise) (i) There exists a measurable function $g^* : \mathcal{W}^c \rightarrow [0, 1]$ and a noise term ε_T such that $T = g^*(\mathbf{W}^c) + \varepsilon_T$, where ε_T is independent of \mathbf{W} , $\mathbb{E}[\varepsilon_T] = 0$, and $\mathbb{E}[\varepsilon_T^2] < \infty$. (ii) There exists a measurable function $Q_T^* : \{0, 1\} \times \mathcal{W}^c \rightarrow \mathbb{R}$ and a noise term ε_Y such that $Y = Q_T^*(\mathbf{W}^c) + \varepsilon_Y$, where ε_Y is independent of (T, \mathbf{W}) , $\mathbb{E}[\varepsilon_Y] = 0$, and $\mathbb{E}[\varepsilon_Y^2] < \infty$. (iii) The exogenous noise terms ε_T and ε_Y are independent.

This assumption coincides with classical additive-noise models under which residual independence characterizes sufficiency of the conditioning set.

Under Assumption (A4), if the selected token subset $\tilde{\mathbf{W}}$ is sufficient for confounding adjustment, then the residual dependence between treatment and outcome vanishes, and HSIC provides a principled measure of this property, as detailed in the following proposition with proof provided in Section A.2 of supplementary article.

Proposition 3.1. *Let $\tilde{\mathbf{W}} \subseteq \mathbf{W}$ be any candidate subset. Define $g(\tilde{\mathbf{W}}) = \mathbb{E}[T | \tilde{\mathbf{W}}]$ and $Q_t(\tilde{\mathbf{W}}) = \mathbb{E}[Y | T = t, \tilde{\mathbf{W}}]$, as well as residuals $r_T = T - g(\tilde{\mathbf{W}})$ and $r_Y = Y - Q_T(\tilde{\mathbf{W}})$, for treatment and outcome respectively. Let $D(\tilde{\mathbf{W}}) = \text{HSIC}(r_T, r_Y)$ be the population-level HSIC computed with characteristic and bounded kernels under finite second moments. Suppose Assumptions (A1), (A3), and (A4), hold. Then,*

$$(Y(0), Y(1)) \perp T | \tilde{\mathbf{W}} \implies D(\tilde{\mathbf{W}}) = 0.$$

Contrapositively, if the residual HSIC is positive, then $\tilde{\mathbf{W}}$ is not sufficient, i.e.,

$$D(\tilde{\mathbf{W}}) > 0 \implies (Y(0), Y(1)) \not\perp T | \tilde{\mathbf{W}}.$$

Remark. We compute HSIC using characteristic kernels. For the binary or nearly discrete treatment residual r_T , a linear kernel $k_T(u, v) = u^\top v$ is sufficient and avoids introducing an arbitrary bandwidth. For the continuous outcome residual r_Y , we employ a Gaussian RBF kernel $k_Y(u, v) = \exp(-\|u - v\|^2/2\sigma_Y^2)$, which captures nonlinear dependence and remains characteristic under mild

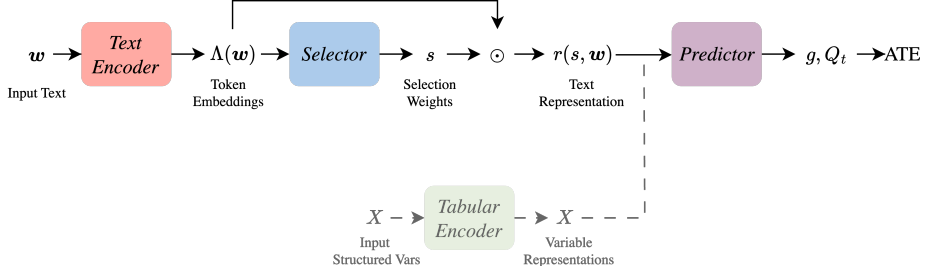


Figure 3: The Confounding-Aware Token Rationalization (CATR) framework (with multimodal extension). The main pipeline (solid blocks) implements selective rationalization for text-only inputs. The semi-transparent dashed components illustrate the extension to tabular covariates, showing that our approach naturally adapts to multi-modal settings.

moment conditions. The bandwidth σ_Y is set by the median heuristic $\sigma_Y^2 = \text{median}\{\|r_{Y,i} - r_{Y,j}\|^2\}$. This choice follows common practice in independence testing and balances bias and variance in the HSIC estimate.

Remark. Residual HSIC provides a *falsification test*: residual dependence indicates that the subset $\tilde{\mathbf{W}}$ fails to block all confounding paths. This use follows HSIC-based independence testing (Gretton et al., 2005, 2007) and related kernel (conditional) independence tests applied in feature selection and causal discovery (Song et al., 2012; Zhang et al., 2011; Strobl et al., 2019). Following the logic of falsification checks in observational studies (e.g., Pearl, 1995; Faller et al., 2024; Karlsson and Krijthe, 2025), the test is necessary but not sufficient for unconfoundedness: $D(\tilde{\mathbf{W}}) = 0$ does not prove unconfoundedness (which is untestable), but $D(\tilde{\mathbf{W}}) > 0$ refutes it, thus serving as a conservative diagnostic. While Proposition 3.1 and the above remark establish the diagnostic role of residual HSIC with g and Q_t defined as the true conditional expectations, we later incorporate it as a regularization term in the training objective (Section 4). In practice, neural estimators \hat{g} and \hat{Q}_t approximate these mappings within bounded error under regularity conditions and networks of sufficient capacity (see Theorem 5.1). This penalization encourages approximate residual independence during optimization, thereby balancing sufficiency and overlap in finite samples.

4 Methodology

In this section, we formally introduce the Confounding-Aware Token Rationalization (CATR) framework, which integrates HSIC-based residual dependence into token-level rationalization to select subsets of text that are sufficient for confounder adjustment and mitigate observational-level positivity violations. We detail the learning architecture, the main objective function, and an extension

to multimodal data. The overall framework is illustrated in Figure 3, and the training procedure is summarized in Algorithm 1.

4.1 Learning Architecture

Build upon the standard rationalization paradigm (see e.g., [Jain et al., 2020](#); [Antognini and Faltings, 2021](#)), our CATR framework consists of a selector $S(\cdot)$, and predictors $g(\cdot)$ and $\{Q_t(\cdot)\}_{t \in \{0,1\}}$. For each observed text \mathbf{w}_i , the selector $S_\theta(\cdot)$ produces a token-level mask $s_i = S_\theta(\mathbf{w}_i) \in [0, 1]^{L_i}$ parameterized by θ . During training, s_i is drawn from a relaxed Bernoulli distribution to introduce stochasticity and encourage exploration of alternative subsets; at evaluation time, we instead use deterministic selection probabilities. The resulting selected subsequence is formed as $\tilde{\mathbf{w}}_i = s_i \odot \mathbf{w}_i$, where \odot denotes elementwise multiplication. Given selected $\tilde{\mathbf{w}}_i$, the predictor network h_ϕ (parameterized by ϕ) produces the estimated propensity score $\hat{g}(\tilde{\mathbf{w}}_i)$ and estimated conditional outcomes $\{\hat{Q}_t(\tilde{\mathbf{w}}_i)\}_{t \in \{0,1\}}$. These estimates serve as plug-in components for standard estimators of ATE τ . The full learning architecture is presented in Figure 3.

Conceptually, the architecture parallels DragonNet ([Shi et al., 2019](#)), except that the input representation $\tilde{\mathbf{w}}$ is itself learnable through the selector $S_\theta(\cdot)$ rather than fixed. This design enables token-level control of confounding adjustment. The resulting token subsets provide interpretable evidence of which linguistic features contribute most to confounding adjustment, facilitating both qualitative inspection and quantitative evaluation.

4.2 Objective Function

Given a training dataset $\mathcal{D} = \{(\mathbf{w}_i, t_i, y_i)\}_{i=1}^n$, CATR learns the selector and predictors by minimizing the following objective:

$$\min_{\theta, \phi} \frac{1}{n} \sum_{i=1}^n \left[\mathcal{L}_{\text{sup},i} + \mu \mathcal{R}_{\text{sparse}}(s_i) + \gamma \text{HSIC}(r_{T,i}, r_{Y,i}) \right], \quad (1)$$

where $s_i = S_\theta(\mathbf{w}_i)$ is the selection mask, and $\mu, \gamma > 0$ control the trade-off among predictive accuracy, sparsity, and residual independence. The loss consists of three components with training procedure summarized in Algorithm 1:

(i) Supervised loss.

$$\mathcal{L}_{\text{sup},i} = \text{CE}(t_i, \hat{g}_\phi(\tilde{\mathbf{w}}_i)) + \text{CE}(y_i, \hat{Q}_{t_i, \phi}(\tilde{\mathbf{w}}_i)),$$

which trains the propensity score predictor \hat{g} and the potential outcome predictors $\{\hat{Q}_t\}_{t \in \{0,1\}}$, where CE means the cross-entropy loss.

(ii) Sparsity regularization. $\mathcal{R}_{\text{sparse}}(s_i)$ is a general regularization term that encourages compact token subsets. Depending on the desired sparsity level, it can take various forms such as Kullback–Leibler divergence to a Bernoulli prior $\text{KL}(s_i \parallel \pi)$ for enforcing a token budget π , entropy regularization $-\sum_j s_{ij} \log s_{ij}$

Algorithm 1 Confounding-Aware Token Rationalization (CATR)

- 1: **Input:** dataset $\mathcal{D} = \{(\mathbf{w}_i, t_i, y_i)\}_{i=1}^n$; temperature η ; prior budget π ; loss weights (μ, γ)
 - 2: Split \mathcal{D} into training and validation sets
 - 3: Initialize selector $S(\cdot)$, predictor $g(\cdot)$, and $\{Q_t(\cdot)\}_{t \in \{0,1\}}$
 - 4: **while** not converged **do**
 - 5: Sample minibatch $\{(\mathbf{w}_i, t_i, y_i)\}_{i=1}^m \sim \mathcal{D}_{\text{train}}$
 - 6: Compute selection score $a_i = S_\theta(\mathbf{w}_i)$
 - 7: Sample relaxed gates $s_{ij} \sim \text{RelaxedBernoulli}(\eta, a_i)$ to form a differentiable binary mask
 - 8: Apply mask to obtain subsequence $\tilde{\mathbf{w}}_i = s_i \odot \mathbf{w}_i$
 - 9: Predictor outputs estimated propensity score $\hat{g}(\tilde{\mathbf{w}}_i)$ and conditional mean outcomes $\{\hat{Q}_t(\tilde{\mathbf{w}}_i)\}_{t \in \{0,1\}}$
 - 10: Form residuals $r_{T,i} = t_i - \hat{g}_i$, $r_{Y,i} = y_i - \hat{Q}_{t_i,i}$
 - 11: Compute loss in Equation (1)
 - 12: Update model parameters via stochastic gradient descent
 - 13: **end while**
 - 14: **Output:** trained selector $S(\cdot)$, predictors $g(\cdot)$ and $\{Q_t(\cdot)\}_{t \in \{0,1\}}$
-

for promoting confident selections, or norm-style penalties for direct sparsity control. This flexibility allows practitioners to adjust the strength and style of sparsity according to their interpretability or computational preferences. In all experiments, we use entropy regularization to avoid additional hyperparameter tuning.

(iii) HSIC penalty. HSIC($r_{T,i}, r_{Y,i}$) measures residual dependence between treatment and outcome, encouraging the selected subset to retain sufficient confounding information. While Proposition 3.1 establishes its diagnostic role, its inclusion here serves as a soft regularizer that penalizes residual dependence during training. Minimizing empirical HSIC does not guarantee perfect unconfoundedness, but it guides the learned representation toward subsets that approximate conditional independence. In practice, HSIC is computed across minibatches; we present it here in a simplified per-sample form for clarity.

Taken together, the objective balances accuracy, sparsity, and sufficiency for valid causal adjustment: the supervised loss ensures predictive fidelity, the sparsity regularizer enforces concise token subsets under user-defined constraints, and the HSIC term promotes residual independence, thereby stabilizing causal effect estimation. The hyperparameter selection and implementation details are provided in Section C of supplementary article.

With learnt propensity score predictor \hat{g} and the conditional mean outcome predictors $\{\hat{Q}_t\}_{t \in \{0,1\}}$, we consider common ATE estimators for τ , including outcome regression (OR) (Pearl, 2000), inverse propensity weighting (IPW) (Rosenbaum and Rubin, 1983), and augmented IPW (AIPW) (Bang and

Robins, 2005):

$$\hat{\tau}_{OR} = \frac{1}{n} \sum_{i=1}^n \left[\hat{Q}_{1,i} - \hat{Q}_{0,i} \right], \quad \hat{\tau}_{IPW} = \frac{1}{n} \sum_{i=1}^n \left[\frac{t_i y_i}{\hat{g}_i} - \frac{(1-t_i)y_i}{1-\hat{g}_i} \right], \quad (2)$$

$$\hat{\tau}_{AIPW} = \frac{1}{n} \sum_{i=1}^n \left[\frac{t_i(y_i - \hat{Q}_{1,i})}{\hat{g}_i} + \hat{Q}_{1,i} - \frac{(1-t_i)(y_i - \hat{Q}_{0,i})}{1-\hat{g}_i} - \hat{Q}_{0,i} \right], \quad (3)$$

where \hat{g}_i and $\hat{Q}_{t,i}$ denote the estimated propensity score and conditional outcome for unit i . Recent theoretical results (Farrell et al., 2021) show that, under mild smoothness and regularization conditions, neural network estimators of nuisance functions can achieve desirable convergence rates and admit non-asymptotic error bounds, as well as distributions for plug-in treatment effect estimators. Since the HSIC penalty regularizes (\hat{g}, \hat{Q}_t) without altering the estimating equations, our method fits naturally into this framework. Under standard regularity and rate conditions for nuisance estimators, the AIPW estimator based on CATR retains the asymptotic properties of the classical semiparametric estimator.

4.3 Extension: Multimodal Data

While our main method is developed for text-only settings, many applications also include well-curated structured covariates. In such cases, text can serve as an important supplementary source of confounding information (see motivating example in Table 1). We extend our framework to jointly handle textual and structured data by encoding tabular covariates into dense vectors of the same dimension as text embeddings. We follow the strategy of Ebrahimi et al. (2023). A cross-attention module then fuses the two representations into a single vector, which is passed to the causal inference model (Figure 3). In this end-to-end differentiable architecture, the token selection mechanism continues to operate on the text encoder output, while the fused representation allows joint adjustment for both text and structured covariates without modifying the core architecture, thereby highlighting the flexibility of our approach. We view this as an extension to our method rather than a primary methodological contribution. Nevertheless, developing more efficient integration strategies for structured and unstructured data in causal inference remains a promising future direction.

5 Theoretical Analysis

This section establishes the statistical properties of the proposed CATR framework. We derive the nonasymptotic error bounds for the neural estimators of the nuisance functions, and establish the \sqrt{n} -consistency and asymptotic normality of the resulting AIPW estimator. All proofs are provided in Section A of supplementary article.

5.1 Nonasymptotic Error Bound of Neural Network Approximation

We begin by introducing a set of regularity conditions required for our theoretical results.

Assumption (A5) (Regularity of data and representation) The treatment $T \in \{0, 1\}$ and outcome $Y \in [-M, M]$ for some $M > 0$. The observed text \mathbf{W} is encoded by a pretrained model into a bounded, continuous-valued feature vector $\mathbf{x} = \Lambda(\mathbf{W}) \in [-1, 1]^d$, whose distribution admits a bounded density on $[-1, 1]^d$, where d is the encoder output dimension.

Assumption (A6) (Smoothness) For each target function $f \in \{g, Q_0, Q_1\}$, assume that f lies in a Sobolev ball $\mathcal{W}^{\beta, \infty}([-1, 1]^d)$ with smoothness $\beta > 0$, i.e.,

$$f(\mathbf{x}) \in \mathcal{W}^{\beta, \infty}([-1, 1]^d) := \left\{ f : \max_{|\alpha| \leq \beta} \text{ess sup}_{\mathbf{x} \in [-1, 1]^d} |D^\alpha f(\mathbf{x})| \leq 1 \right\},$$

where $\alpha = (\alpha_1, \dots, \alpha_d)$, $|\alpha| = \sum_j \alpha_j$, and $D^\alpha f$ denotes the weak derivative.

Assumption (A7) (Regularity of penalization terms) The regularization terms $\mathcal{R}_{\text{sparse}}$ and HSIC are nonnegative and uniformly bounded.

In language-based settings, these assumptions are generally mild and reasonable. Pretrained encoders map semantically similar texts to nearby continuous embeddings within a bounded region, so the representation distribution admits a bounded density, satisfying Assumption (A5). Moreover, linguistic properties vary smoothly in the embedding space. Small semantic or syntactic changes in text typically lead to gradual changes in treatment propensity or conditional outcome expectation. Hence, it is natural to assume that the underlying functions $f \in \{g, Q_0, Q_1\}$ are smooth, as required by Assumption (A6). Assumption (A7) is mild and typically holds in practice. For HSIC, commonly used kernels, such as Gaussian RBF or cosine kernels, are bounded in $[0, 1]$, so the resulting dependence measure is nonnegative and finite. For sparsity regularization, KL- or entropy-based penalties are also bounded on compact domains ($s_i \in [0, 1]$). Hence both regularization terms naturally satisfy this assumption.

Under the above assumptions, we establish the nonasymptotic error bound for deep MLP-ReLU network approximation following the framework of [Farrell et al. \(2021\)](#).

Theorem 5.1. *Suppose Assumptions (A5)–(A7) hold. Let \hat{f} be the minimizer of the joint objective (1), with fixed penalty weights $\mu, \gamma = O(1)$ independent of n . Then, for an MLP-ReLU network class with width $H \asymp n^{\frac{d}{2(\beta+d)}}$ $\log^2 n$ and depth $D \asymp \log n$, there exists $C > 0$ such that, with probability at least $1 - \exp(-n^{\frac{d}{\beta+d}} \log^8 n)$,*

$$\|\hat{f} - f_*\|_{L_2(P_X)}^2 \leq C \left(n^{-\frac{\beta}{\beta+d}} \log^8 n + \frac{\log \log n}{n} \right),$$

where f represents either g or Q_t , f_* denotes the true target function.

Theorem 5.1 extends the standard consistency result in Farrell et al. (2021) to the case of jointly estimated models with additional regularization. Since both $\mathcal{R}_{\text{sparse}}$ and HSIC are bounded and weighted by fixed constants, the penalized objective can be viewed as a constrained version of the unpenalized empirical risk minimization; therefore, the convergence rate $n^{-\beta/(\beta+d)}$ remains unchanged. Intuitively, the HSIC term promotes independence between treatment and outcome representations, and the sparsity term encourages concise rationales, but neither alters the statistical order of estimation error. While d corresponds to the full embedding size, selective rationalization reduces the effective input complexity by removing spurious or irrelevant components, thereby improving convergence in practice. Hence, reducing the dimensionality of text by selecting smaller subsets of tokens can improve the propensity estimation accuracy.

5.2 Statistical Inference

We first show the consistency and convergence of nuisance estimators.

Theorem 5.2. *Suppose Assumptions (A1)–(A7) hold, and the nonasymptotic bound in Theorem 5.1 holds, then, the estimators \hat{g} and \hat{Q}_t satisfy, for $t \in \{0, 1\}$:*

- (a) $\mathbb{E}_n[(\hat{g}(\mathbf{w}_i) - g(\mathbf{w}_i))^2] = o_P(1)$, $\mathbb{E}_n[(\hat{Q}_t(\mathbf{w}_i) - Q_t(\mathbf{w}_i))^2] = o_P(1)$;
- (b) $\mathbb{E}_n[(\hat{Q}_t(\mathbf{w}_i) - Q_t(\mathbf{w}_i))^2] \mathbb{E}_n[(\hat{g}(\mathbf{w}_i) - g(\mathbf{w}_i))^2] = o_P(n^{-1})$;
- (c) $\mathbb{E}_n[(\hat{Q}_t(\mathbf{w}_i) - Q_t(\mathbf{w}_i))(t_i - g(\mathbf{w}_i))] = o_P(n^{-1/2})$.

Let $\hat{\psi}_t$ denote the plug-in orthogonal score, defined for each treatment as

$$\hat{\psi}_1 = \frac{t_i}{\hat{g}(\mathbf{w}_i)} \{y_i - \hat{Q}_1(\mathbf{w}_i)\} + \hat{Q}_1(\mathbf{w}_i), \quad \hat{\psi}_0 = \frac{1 - t_i}{1 - \hat{g}(\mathbf{w}_i)} \{y_i - \hat{Q}_0(\mathbf{w}_i)\} + \hat{Q}_0(\mathbf{w}_i).$$

If $\hat{g}(\mathbf{w}_i)$ is bounded away from 0 and 1, then the empirical mean and second moment of the estimated score converge to their population counterparts:

$$\sqrt{n} \mathbb{E}_n[\hat{\psi}_t - \psi_t] = o_P(1), \quad \frac{\mathbb{E}_n[(\hat{\psi}_t)^2]}{\mathbb{E}_n[(\psi_t)^2]} - 1 = o_P(1).$$

Theorem 5.2 emphasizes the importance of observational-level positivity for the validity of convergence estimation. When the observational-level positivity is violated, the inverse weighting terms $1/\hat{g}(\mathbf{w})$ and $1/\{1 - \hat{g}(\mathbf{w})\}$ may diverge, causing the orthogonal scores to have unbounded variance. Positivity ensures that both the empirical process and the remainder terms in Theorem 5.2 remain well behaved, thereby guaranteeing finite-variance estimation of treatment effects. Building on these properties, we now analyze the convergence and asymptotic normality of the treatment effect estimators. We formalize these results below.

Theorem 5.3. *Suppose Assumptions (A1)–(A7) hold. Assume that the convergence rates in Theorem 5.2 hold. Define $\hat{\tau}_{\text{IPW}}$ and $\hat{\tau}_{\text{AIPW}}$ as in Equations (2) and (3). Let τ denote the ground truth ATE.*

- (a) (Consistency) $\hat{\tau}_{\text{IPW}}, \hat{\tau}_{\text{AIPW}} \xrightarrow{P} \tau$.
- (b) (AIPW asymptotic normality) If we further assume the nuisance estimators \hat{g} and \hat{Q}_t satisfy the product-rate condition

$$\|\hat{g} - g\|_{L_2(P_{\mathbf{w}})} \cdot \|\hat{Q}_t - Q_t\|_{L_2(P_{\mathbf{w}})} = o_P(n^{-1/2}),$$

then

$$\sqrt{n}(\hat{\tau}_{\text{AIPW}} - \tau) \rightsquigarrow \mathcal{N}(0, V^*), \quad V^* = \text{Var}(\hat{\psi}_1 - \hat{\psi}_0).$$

Theorem 5.3 shows that while both IPW and AIPW estimators are consistent under overlap, only AIPW achieves \sqrt{n} -asymptotic normality under the weaker product-rate condition, which aligns with our experimental results in Section 6.

6 Empirical Experiments

In this section, we evaluate the proposed CATR using both controlled semi-synthetic studies and a real-world analysis of the MIMIC-III sepsis cohort. Our empirical objectives are threefold: (i) to assess whether CATR identifies token subsets that preserve essential confounding information; (ii) to examine its ability to mitigate observational-level positivity violations and thereby stabilize causal estimators; and (iii) to benchmark its performance against existing text-based causal inference methods. We begin with a semi-synthetic design that permits evaluation of estimation accuracy relative to the true ATE, and then investigate CATR in a fully observational clinical setting to assess its practical utility.

6.1 Synthetic Experiment

We conduct semi-synthetic experiments with known treatment effects, using the MIMIC-III v1.4 database (Johnson et al., 2016). We focus on a subset of ICU patients with sepsis. For each patient i , we extract the earliest physician note within eight hours of admission, which serves as the high-dimensional textual confounder \mathbf{w}_i . To allow for unbiased benchmarking of causal estimators under a realistic but controlled setting, we simulate treatment assignments and outcomes directly from the clinical notes. We first construct a binary indicator based on the presence of infection-related keywords (*shock/hypotension*, *infection/sepsis/pneumonia*). This indicator is transformed through nonlinear mappings to generate both the propensity score and the potential outcome functions:

$$t_i \sim \text{Bernoulli}(g(\mathbf{w}_i)), \quad y_i = Q_{t_i}(\mathbf{w}_i) + \varepsilon_i.$$

Treatment assignments t_i are sampled from the resulting propensity score distribution, and outcomes y_i are drawn from the corresponding potential outcome models. This design preserves the realistic linguistic and statistical structure of clinical text while allowing the true ATE to be computed as $\tau_{\text{true}} = \mathbb{E}[Y(1) - Y(0)]$. More details on synthetic data construction is provided in Section B of supplementary article.

Table 2: Comparison of ATE estimation and positivity diagnostics across methods.

Method	Estimator	ATE metrics over replications ^a				PS Quality	
		Mean(Bias)	SD($\widehat{\text{ATE}}$)	Avg SE	C.I. Coverage ^b	ESS Ratio	Clip. Frac. ^c
TARNet ^d	OR	0.1448	0.1780	0.0219	21.0%	—	—
CFRNet ^d	OR	0.1425	0.1733	0.0215	20.5%	—	—
DragonNet	OR	0.1600	0.1989	0.0201	16.5%	0.2716	28.89%
	IPW	1.1880	1.0440	0.6170	35.5%		
	AIPW	0.3200	0.4383	0.3289	85.0%		
CausalBERT	OR	0.1943	0.2434	0.0229	13.5%	0.2656	30.96%
	IPW	1.3928	1.1039	0.6485	48.5%		
	AIPW	0.3506	0.4747	0.3490	87.5%		
CATR	OR	0.1863	0.2306	0.0157	10.0%	0.3097	10.74%
	IPW	0.7038	0.8447	0.4938	76.0%		
	AIPW	0.2610	0.3165	0.2649	90.0%		

^a Experiments are replicated for 200 times and bootstrap $B = 1000$.

^b Confidence level is 95%.

^c Clipping threshold is 0.03/0.97.

^d TARNet and CFRNet do not explicitly estimate the propensity score, so only OR estimation of ATE is reported.

We compare our method against four baseline methods, including TARNet/CFRNet (Shalit et al., 2017), DragonNet (Shi et al., 2019), and CausalBERT (Veitch et al., 2020). For all models, we use the officially released source code when available, or reimplement them using the optimal hyperparameter settings reported in their respective papers. To ensure comparability, all text-based models use the same encoder backbone, ClinicalBERT (Wang et al., 2023; Liu et al., 2025), to generate embeddings. Implementation uses the Adam optimizer with early stopping based on validation loss. Data are randomly split into training, validation, and test sets in a 25:6:6 ratio, which are used respectively for model fitting, early stopping, and final evaluation. Hyperparameter settings generally follow those used in the original implementations of each baseline to ensure fair comparison. See more details in Section C of supplementary article.

Each model produces estimates of the conditional outcome functions $Q_t(\mathbf{w})$ and the propensity score $g(\mathbf{w})$, which are then used to compute three standard ATE estimators, OR, IPW, and AIPW, as defined in Equations (2)-(3). Each model is evaluated over $R = 200$ independent replications, each producing three ATE estimators (OR, IPW, and AIPW) based on newly sampled treatment and outcome assignments. For each replication–estimator pair, we compute the point estimate $\widehat{\tau}_r$ and its bootstrap standard deviation $\widehat{\text{SE}}_{r,e}$ using $B = 1000$ resamples, and construct the 95% confidence interval $[\widehat{\tau}_r \pm 1.96 \widehat{\text{SE}}_r]$ under approximate normality of the bootstrap distribution. Across replications, we report:

- **Mean(|Bias|)**: $\frac{1}{R} \sum_{r=1}^R |\widehat{\tau}_r - \tau_{\text{true}}|$;
- **SD($\widehat{\text{ATE}}$)**: empirical standard deviation of $\widehat{\tau}_r$ over replications;
- **Avg SE**: mean of the bootstrap standard deviations, $\frac{1}{R} \sum_{r=1}^R \widehat{\text{SE}}_r$;
- **C.I. Coverage (95%)**: proportion of confidence intervals that cover the true ATE, $\frac{1}{R} \sum_{r=1}^R \mathbb{I}\{\tau_{\text{true}} \in [\widehat{\tau}_r \pm 1.96 \widehat{\text{SE}}_r]\}$;

- **ESS Ratio:** ratio of the estimated effective sample size to its oracle counterpart, $\text{ESS}_{\text{ratio}} = \text{ESS}(\hat{w})/\text{ESS}(w^*)$, where $\text{ESS}(w) = (\sum_i w_i)^2 / \sum_i w_i^2$ and w^* denotes the true inverse-propensity weights. Values closer to 1 indicate better recovery of the effective sample size and stronger empirical overlap.
- **Clipping Frac.:** fraction of units with estimated propensity scores $\hat{g}_i \notin [0.03, 0.97]$, indicating observational-level positivity violations.

For each method, the ESS ratio and clipping fraction are reported once, averaged across all replications, while ATE metrics are reported separately for OR, IPW, and AIPW estimators. A lower mean absolute bias and standard deviation, together with higher coverage and ESS ratio, reflect more accurate and stable causal effect estimation with improved treatment overlap.

As shown in Table 2, CATR noticeably improves empirical overlap and stability compared to all baselines. By reducing the fraction of extreme propensity scores and increasing the effective sample size, it alleviates observational-level positivity violations that commonly arise in text-based confounding adjustment. This improvement translates into lower bias and variance for both IPW and AIPW estimators, together with higher confidence interval coverage, especially for IPW estimator which purely relies on the propensity modeling. In contrast, baseline models such as DragonNet and CausalBERT exhibit unstable inverse weights and wide confidence intervals due to overfitting and redundant token dependencies. Taken together, these results indicate that the HSIC-guided sparse rationalization in CATR enhances both statistical efficiency and interpretability by filtering out spurious linguistic correlations while preserving true confounding signals.

Table 3 further demonstrates the effectiveness of our approach. For the IPW estimator, the improvements brought by CATR are substantial: removing the HSIC term leads to a marked increase in both bias and variance, along with a higher clipping fraction, underscoring how critical the residual-independence constraint is for recovering accurate propensities. When both HSIC and sparsity are removed, the degradation becomes even more severe, with large IPW bias and unstable confidence intervals—highlighting the extent to which CATR mitigates positivity violations. For the AIPW estimator, CATR not only achieves higher coverage rates, but does so while simultaneously reducing both the standard deviation and the standard error, indicating more stable inference and more reliable uncertainty quantification. Together, these results show that CATR consistently strengthens estimation stability, confirming the overall effectiveness of the method.

Figure 4 compares the top-20 important words selected with and without HSIC regularization. When a word is tokenized into multiple subword units, we define its overall importance score as the average of the individual token-level importance scores. Without the HSIC constraint, most of the selected tokens appear only once and are largely unrelated to the pre-specified confounding words. This pattern indicates that the model tends to capture spurious correlations rather than meaningful causal signals. By contrast, when HSIC is incorporated,

Table 3: CATR ablation study.

Method	Estimator	ATE metrics over replications ^a				PS Quality	
		Mean(Bias)	SD(\widehat{ATE})	Avg SE	C.I. Coverage ^b	ESS Ratio	Clip. Frac. ^c
Full CATR	OR	0.1863	0.2306	0.0157	10.0%	0.3097	10.74%
	IPW	0.7038	0.8447	0.4938	76.0%		
	AIPW	0.2610	0.3165	0.2649	90.0%		
-HSIC	OR	0.1504	0.1863	0.0153	10.5%	0.2895	17.36%
	IPW	0.9781	0.9467	0.5696	67.5%		
	AIPW	0.2781	0.3347	0.3035	90.0%		
-Sparsity	OR	0.1611	0.1985	0.0200	17.0%	0.2699	29.55%
	IPW	1.2408	1.0830	0.6230	51.0%		
	AIPW	0.3212	0.4383	0.3327	89.5%		

^a Experiments are replicated for 200 times and bootstrap $B = 1000$.

^b Confidence level is 95%.

^c Clipping threshold is 0.03/0.97.

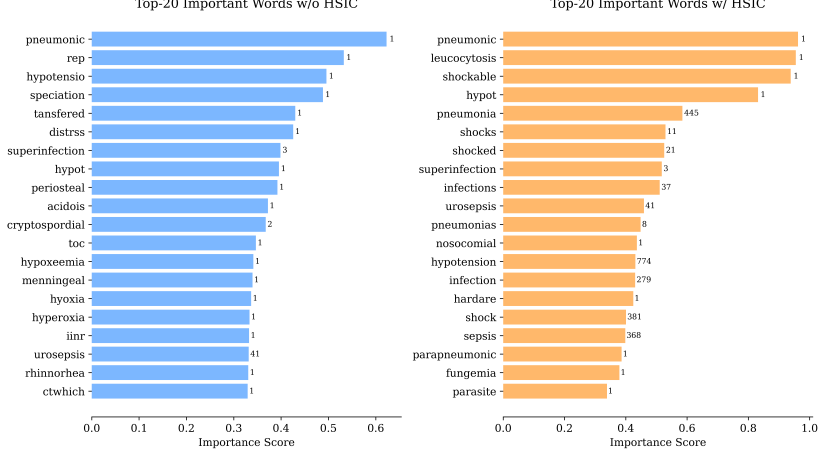


Figure 4: Comparison of importance score distributions with and without HSIC regularization.

this behavior is substantially mitigated: all manually defined confounding words (*sepsis*, *infection*, *pneumonia*, *shock*, *hypotension*) are successfully recalled, along with multiple variants sharing the same morphological roots (e.g., *shocked*, *pneumonic*). By penalizing the residual dependence between T and Y under the text representation, the model avoids mistaking coincidental co-occurrences for discriminative signals, and learns the underlying causal mechanism and enhances the interpretability of black-box representations.

6.2 Real Data Analysis

To complement the synthetic experiments, we analyze the same cohort from MIMIC-III database as in the simulation, with naturally occurring treatment and outcomes. Treatment is defined as intravenous (IV) fluid therapy and outcome is defined as ICU readmission. For each patient, we extract both physician notes and structured covariates (42 variables including demographics, comorbidities,

Table 4: Comparison of ATE and positivity diagnostics on real MIMIC-III datasets.

	ATE (std)			PS Quality	
	OR	IPW	AIPW	ESS Ratio	Clipping Frac. ^d
Structured-only	-0.0687 (0.0085)	-0.0005 (0.1054)	-0.0427 (0.0942)	0.2113	8.18%
Multi-modal (w/o. CATR)	0.0465 (0.0054)	0.1178 (0.1923)	-0.1209 (0.1541)	0.2766	20.44%
Multi-modal (w. CATR)	-0.1137 (0.0020)	-0.0490 (0.0569)	-0.0256 (0.0414)	0.8522	0%

^a Reported ATE is calculated after clipping at a threshold of 0.05. Standard deviations (std) are based on 30 bootstrap replicates of ATE estimation.

^d The clipping is conducted at 0.03/0.97.

vitals, and labs, provided in Section D of supplementary article). This setting evaluates our multimodal extension (Section 4.3), which integrates structured variables and unstructured text to model confounding. The analysis allows us to assess whether our framework remains effective in practical applications with real treatment assignments and outcomes.

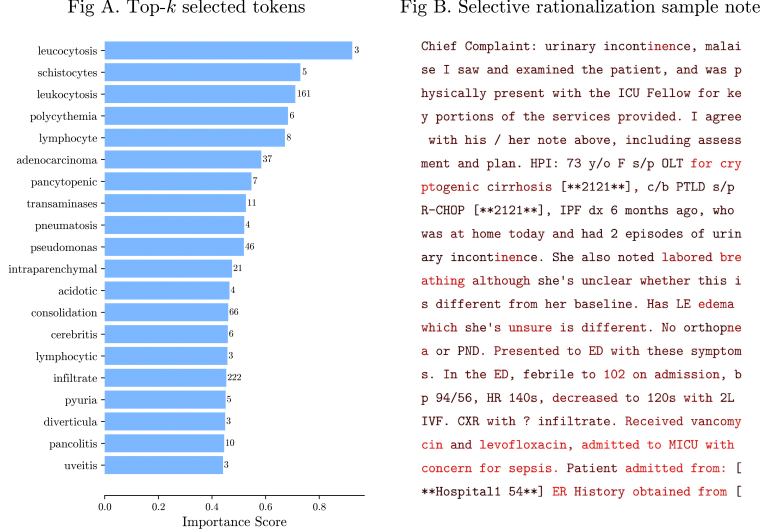


Figure 5: Fig. A shows top- k selected tokens that are medically informative. Fig. B visualizes the selective rationalization output with color-encoded selection importance scores.

We compare three adjustment strategies: structured-only, multimodal without CATR, and multimodal with CATR. For the structured-only setting, we use logistic regression for both propensity and outcome modeling. For the multimodal setting, we adopt the architecture described in Section 4.3. We evaluate the ATE estimates and their bootstrap standard deviations over 1,000 bootstrap resamples, and also report prediction accuracy and propensity score quality. As shown in Table 4, incorporating text substantially improves prediction accuracy, confirming that textual information provides additional confounding-relevant signals. The multimodal model with CATR yields the most stable ATE estimates across OR, IPW, and AIPW, with higher ESS and lower clipping fractions. Moreover, with

multimodal data and selective rationalization, the magnitudes and directions of estimated causal effects align more closely across estimators, indicating improved stability. The AIPW estimate is -2.56% with a smaller standard deviation, suggesting reduced variance and stronger agreement among estimators. Overall, IV treatment shows no significant causal effect on ICU readmission among sepsis patients, consistent with recent studies that question uniform benefits and highlight heterogeneous subgroup effects (Lung et al., 2023; Sivapalan et al., 2023).

Beyond quantitative results, Figure 5 shows that CATR selects clinically meaningful tokens, such as terms indicating infections, organ dysfunction, or other severity markers that influence both treatment decisions and outcomes. These include keywords like “sepsis”, “infection”, and “hypotension”, as well as descriptors of patient condition (e.g., “labored breathing”, “unsure”). Such terms plausibly serve as confounders linking IV administration and patient prognosis.

In summary, CATR improves empirical overlap, stabilizes propensity weighting, and enhances interpretability without relying on ad hoc trimming. When combined with structured covariates, these benefits are further amplified, producing narrower confidence intervals and more robust ATE estimates.

7 Conclusion

We propose a unified framework for causal effect estimation when text is used to adjust for confounding. Our approach explicitly targets *observational-level positivity violations*, which occur when high-dimensional textual confounders induce near-deterministic treatment assignment despite positivity holding at the latent level. To address this, we incorporate selective rationalization that identifies a compact yet sufficient textual rationale set for treatment assignment, yielding representations with improved overlap. Empirically, this design improves ATE estimation in experiments, highlighting the potential of our approach for robust causal inference from natural language.

Future work could strengthen causal interpretability by integrating counterfactual reasoning to explicitly enforce necessity and sufficiency of selected tokens. In addition, the framework can be naturally combined with post-hoc adjustment methods, such as temperature scaling, beta or histogram calibration, and covariate balancing techniques, to further stabilize propensity estimates and reduce residual bias. More broadly, we hope our framework encourages further investigation of how high-dimensional text proxies interact with core causal assumptions such as positivity and unconfoundedness, providing opportunities to refine text-based causal inference in applied domains, including healthcare and policy.

References

- Emily Alsentzer, John Murphy, William Boag, Wei-Hung Weng, Di Jindi, Tristan Naumann, and Matthew McDermott. Publicly available clinical bert embeddings. In *Proceedings of the 2nd clinical natural language processing workshop*, pages 72–78, 2019.
- Diego Antognini and Boi Faltings. Rationalization through concepts. In *Findings of the Association for Computational Linguistics: ACL-IJCNLP 2021*, pages 761–775, 2021.
- Heejung Bang and James M Robins. Doubly robust estimation in missing data and causal inference models. *Biometrics*, 61(4):962–973, 2005.
- Yujia Bao, Shiyu Chang, Mo Yu, and Regina Barzilay. Deriving machine attention from human rationales. In *Proceedings of the 2018 Conference on Empirical Methods in Natural Language Processing*, pages 1903–1913, 2018.
- Jasmijn Bastings, Wilker Aziz, and Ivan Titov. Interpretable neural predictions with differentiable binary variables. In *Proceedings of the 57th Annual Meeting of the Association for Computational Linguistics*, pages 2963–2977, 2019.
- Alexandre Belloni, Victor Chernozhukov, and Christian Hansen. High-dimensional methods and inference on structural and treatment effects. *Journal of Economic Perspectives*, 28(2):29–50, 2014.
- Hengrui Cai, Yixin Wang, Michael Jordan, and Rui Song. On learning necessary and sufficient causal graphs. *Advances in Neural Information Processing Systems*, 36:42148–42160, 2023.
- Stephen R Cole and Miguel A Hernán. Constructing inverse probability weights for marginal structural models. *American journal of epidemiology*, 168(6):656–664, 2008.
- Richard K Crump, V Joseph Hotz, Guido W Imbens, and Oscar A Mitnik. Dealing with limited overlap in estimation of average treatment effects. *Biometrika*, 96(1):187–199, 2009.
- Jacob Devlin, Ming-Wei Chang, Kenton Lee, and Kristina Toutanova. Bert: Pre-training of deep bidirectional transformers for language understanding. In *Proceedings of the 2019 conference of the North American chapter of the association for computational linguistics: human language technologies, volume 1 (long and short papers)*, pages 4171–4186, 2019.
- Sayna Ebrahimi, Sercan Ö Arik, Yihe Dong, and Tomas Pfister. Lanistr: Multi-modal learning from structured and unstructured data. *CoRR*, 2023.
- Naoki Egami, Christian J Fong, Justin Grimmer, Margaret E Roberts, and Brandon M Stewart. How to make causal inferences using texts. *Science Advances*, 8(42):2652, 2022.

- Philipp M Faller, Leena C Vankadara, Atalanti A Mastakouri, Francesco Locatello, and Dominik Janzing. Self-compatibility: Evaluating causal discovery without ground truth. In *International Conference on Artificial Intelligence and Statistics*, pages 4132–4140. PMLR, 2024.
- Max H. Farrell, Tengyuan Liang, and Sanjog Misra. Deep neural networks for estimation and inference. *Econometrica*, 89(1):181–213, 2021. ISSN 0012-9682.
- Amir Feder, Katherine A Keith, Emaad Manzoor, Reid Pryzant, Dhanya Sridhar, Zach Wood-Doughty, Jacob Eisenstein, Justin Grimmer, Roi Reichart, Margaret E Roberts, et al. Causal inference in natural language processing: Estimation, prediction, interpretation and beyond. *Transactions of the Association for Computational Linguistics*, 10:1138–1158, 2022.
- Xinwei Geng, Longyue Wang, Xing Wang, Bing Qin, Ting Liu, and Zhaopeng Tu. How does selective mechanism improve self-attention networks? In *Proceedings of the 58th Annual Meeting of the Association for Computational Linguistics*, pages 2986–2995, 2020.
- Arthur Gretton, Olivier Bousquet, Alex Smola, and Bernhard Schölkopf. Measuring statistical dependence with hilbert-schmidt norms. In *International conference on algorithmic learning theory*, pages 63–77. Springer, 2005.
- Arthur Gretton, Kenji Fukumizu, Choon Teo, Le Song, Bernhard Schölkopf, and Alex Smola. A kernel statistical test of independence. *Advances in neural information processing systems*, 20, 2007.
- Nuno M Guerreiro and André FT Martins. Spectra: Sparse structured text rationalization. In *Proceedings of the 2021 Conference on Empirical Methods in Natural Language Processing*, pages 6534–6550, 2021.
- Paul W. Holland. Statistics and causal inference. *Journal of the American Statistical Association*, 81(396):945–960, 1986. ISSN 01621459, 1537274X. URL <http://www.jstor.org/stable/2289064>.
- Patrik O Hoyer, Dominik Janzing, Joris M Mooij, Jonas Peters, and Bernhard Schölkopf. Nonlinear causal discovery with additive noise models. *Neural Information Processing Systems (NeurIPS)*, 22:689–696, 2009.
- Kexin Huang, Jaan Altosaar, and Rajesh Ranganath. Clinicalbert: Modeling clinical notes and predicting hospital readmission. *arXiv preprint arXiv:1904.05342*, 2019.
- Kosuke Imai and Marc Ratkovic. Covariate balancing propensity score. *Journal of the Royal Statistical Society Series B: Statistical Methodology*, 76(1):243–263, 2014.
- Guido W. Imbens and Donald B. Rubin. *Causal Inference for Statistics, Social, and Biomedical Sciences: An Introduction*. Cambridge University Press, 2015.

- Sarthak Jain, Sarah Wiegreffe, Yuval Pinter, and Byron C Wallace. Learning to faithfully rationalize by construction. In *Proceedings of the 58th Annual Meeting of the Association for Computational Linguistics*, pages 4459–4473, 2020.
- Alistair EW Johnson, Tom J Pollard, Lu Shen, Li-wei H Lehman, Mengling Feng, Mohammad Ghassemi, Benjamin Moody, Peter Szolovits, Leo Anthony Celi, and Roger G Mark. Mimic-iii, a freely accessible critical care database. *Scientific data*, 3(1):1–9, 2016.
- Rickard Karlsson and JH Krijthe. Falsification of unconfoundedness by testing independence of causal mechanisms. In *Forty-second International Conference on Machine Learning*. PMLR, 2025.
- Bryan Keller, Jee-Seon Kim, and Peter M Steiner. Neural networks for propensity score estimation: Simulation results and recommendations. In *Quantitative Psychology Research: The 79th Annual Meeting of the Psychometric Society, Madison, Wisconsin, 2014*, pages 279–291. Springer, 2015.
- Brian K Lee, Justin Lessler, and Elizabeth A Stuart. Weight trimming and propensity score weighting. *PloS one*, 6(3):e18174, 2011.
- Jinhyuk Lee, Wonjin Yoon, Sungdong Kim, Donghyeon Kim, Sunkyu Kim, Chan Ho So, and Jaewoo Kang. Biobert: a pre-trained biomedical language representation model for biomedical text mining. *Bioinformatics*, 36(4):1234–1240, 2020.
- Tao Lei, Regina Barzilay, and Tommi Jaakkola. Rationalizing neural predictions. In *Proceedings of the 2016 Conference on Empirical Methods in Natural Language Processing*, pages 107–117, 2016.
- Fan Li, Kari Lock Morgan, and Alan M Zaslavsky. Balancing covariates via propensity score weighting. *Journal of the American Statistical Association*, 113(521):390–400, 2018.
- Wei Liu, Haozhao Wang, Jun Wang, Ruixuan Li, Chao Yue, and YuanKai Zhang. Fr: Folded rationalization with a unified encoder. *Advances in Neural Information Processing Systems*, 35:6954–6966, 2022.
- Xiaohong Liu, Hao Liu, Guoxing Yang, Zeyu Jiang, Shuguang Cui, Zhaoze Zhang, Huan Wang, Liyuan Tao, Yongchang Sun, Zhu Song, et al. A generalist medical language model for disease diagnosis assistance. *Nature medicine*, 31(3):932–942, 2025.
- Christos Louizos, Uri Shalit, Joris M Mooij, David Sontag, Richard Zemel, and Max Welling. Causal effect inference with deep latent-variable models. *Advances in neural information processing systems*, 30, 2017.

- National Heart Lung, Blood Institute Prevention, and Early Treatment of Acute Lung Injury Clinical Trials Network. Early restrictive or liberal fluid management for sepsis-induced hypotension. *New England Journal of Medicine*, 388(6):499–510, 2023.
- Judea Pearl. On the testability of causal models with latent and instrumental variables. In *Proceedings of the Eleventh conference on Uncertainty in artificial intelligence*, pages 435–443, 1995.
- Judea Pearl, editor. *Causality: models, reasoning and inference, volume 29*. Springer, 2000.
- Jonas Peters, Joris M Mooij, Dominik Janzing, and Bernhard Schölkopf. Causal discovery with continuous additive noise models. *Journal of Machine Learning Research*, 15(1):2009–2053, 2014.
- Jonas Peters, Dominik Janzing, and Bernhard Schölkopf. *Elements of Causal Inference: Foundations and Learning Algorithms*. MIT Press, 2017.
- Margaret E. Roberts, Brandon M Stewart, and Richard A. Nielsen. Adjusting for confounding with text matching. *American Journal of Political Science*, 64:887–903, 2020.
- Paul R Rosenbaum and Donald B Rubin. The central role of the propensity score in observational studies for causal effects. *Biometrika*, 70(1):41–55, 1983.
- Konstantinos I Roumeliotis and Nikolaos D Tsakikas. Chatgpt and open-ai models: A preliminary review. *Future Internet*, 15(6):192, 2023.
- Donald B Rubin. Estimating causal effects of treatments in randomized and nonrandomized studies. *Journal of educational Psychology*, 66(5):688, 1974.
- Lei Sha, Oana-Maria Camburu, and Thomas Lukasiewicz. Learning from the best: Rationalizing predictions by adversarial information calibration. *Proceedings of the AAAI Conference on Artificial Intelligence*, 35(15):13771–13779, May 2021.
- Uri Shalit, Fredrik D Johansson, and David Sontag. Estimating individual treatment effect: generalization bounds and algorithms. In *International conference on machine learning*, pages 3076–3085. PMLR, 2017.
- Claudia Shi, David Blei, and Victor Veitch. Adapting neural networks for the estimation of treatment effects. *Advances in neural information processing systems*, 32, 2019.
- Praleene Sivapalan, Karen L Ellekjaer, Marie K Jessen, Tine S Meyhoff, Maria Cronhjort, Peter B Hjortrup, Jørn Wetterslev, Anders Granholm, Morten H Møller, and Anders Perner. Lower vs higher fluid volumes in adult patients with sepsis: an updated systematic review with meta-analysis and trial sequential analysis. *Chest*, 164(4):892–912, 2023.

- Le Song, Alex Smola, Arthur Gretton, Justin Bedo, and Karsten Borgwardt. Feature selection via dependence maximization. *The Journal of Machine Learning Research*, 13(1):1393–1434, 2012.
- Eric V Strobl, Kun Zhang, and Shyam Visweswaran. Approximate kernel-based conditional independence tests for fast non-parametric causal discovery. *Journal of Causal Inference*, 7(1):20180017, 2019.
- Jin Tian and Judea Pearl. Probabilities of causation: Bounds and identification. *Annals of Mathematics and Artificial Intelligence*, 28(1):287–313, 2000.
- Hugo Touvron, Thibaut Lavril, Gautier Izacard, Xavier Martinet, Marie-Anne Lachaux, Timothée Lacroix, Baptiste Rozière, Naman Goyal, Eric Hambro, Faisal Azhar, et al. Llama: Open and efficient foundation language models. *arXiv preprint arXiv:2302.13971*, 2023.
- Lars van der Laan, Ziming Lin, Marco Carone, and Alex Luedtke. Stabilized inverse probability weighting via isotonic calibration. In *Causal Learning and Reasoning*, pages 139–173. PMLR, 2025.
- Victor Veitch, Dhanya Sridhar, and David Blei. Adapting text embeddings for causal inference. In Jonas Peters and David Sontag, editors, *Proceedings of the 36th Conference on Uncertainty in Artificial Intelligence (UAI)*, pages 919–928. PMLR, 2020.
- Guangyu Wang, Xiaohong Liu, Zhen Ying, Guoxing Yang, Zhiwei Chen, Zhiwen Liu, Min Zhang, Hongmei Yan, Yuxing Lu, Yuanxu Gao, et al. Optimized glycemic control of type 2 diabetes with reinforcement learning: a proof-of-concept trial. *Nature Medicine*, 29(10):2633–2642, 2023.
- Jason Wei, Yi Tay, Rishi Bommasani, Colin Raffel, Barret Zoph, Sebastian Borgeaud, Dani Yogatama, Maarten Bosma, Denny Zhou, Donald Metzler, Ed H. Chi, Tatsunori Hashimoto, Oriol Vinyals, Percy Liang, Jeff Dean, and William Fedus. Emergent abilities of large language models. *Transactions on Machine Learning Research*, 2022. ISSN 2835-8856. URL <https://openreview.net/forum?id=yzkSU5zdwD>. Survey Certification.
- Zach Wood-Doughty, Ilya Shpitser, and Mark Dredze. Challenges of using text classifiers for causal inference. In *Proceedings of the Conference on Empirical Methods in Natural Language Processing. Conference on Empirical Methods in Natural Language Processing*, volume 2018, page 4586, 2018.
- An Yang, Anfeng Li, Baosong Yang, Beichen Zhang, Binyuan Hui, Bo Zheng, Bowen Yu, Chang Gao, Chengan Huang, Chenxu Lv, et al. Qwen3 technical report. *arXiv preprint arXiv:2505.09388*, 2025.
- Mo Yu, Shiyu Chang, Yang Zhang, and Tommi Jaakkola. Rethinking cooperative rationalization: Introspective extraction and complement control. In *Proceedings of the 2019 Conference on Empirical Methods in Natural Language*

Processing and the 9th International Joint Conference on Natural Language Processing (EMNLP-IJCNLP), pages 4094–4103, 2019.

Kun Zhang, Jonas Peters, Dominik Janzing, and Bernhard Schölkopf. Kernel-based conditional independence test and application in causal discovery. In *Proceedings of the Twenty-Seventh Conference on Uncertainty in Artificial Intelligence*, pages 804–813, 2011.

Weijia Zhang, Lin Liu, and Jiuyong Li. Treatment effect estimation with disentangled latent factors. In *Proceedings of the AAAI Conference on Artificial Intelligence*, volume 35, pages 10923–10930, 2021.

Wenbo Zhang, Tong Wu, Yunlong Wang, Yong Cai, and Hengrui Cai. Towards trustworthy explanation: On causal rationalization. In *International Conference on Machine Learning*, pages 41715–41736. PMLR, 2023.

Wayne Xin Zhao, Kun Zhou, Junyi Li, Tianyi Tang, Xiaolei Wang, Yupeng Hou, Yingqian Min, Beichen Zhang, Junjie Zhang, Zican Dong, et al. A survey of large language models. *arXiv preprint arXiv:2303.18223*, 2023.

Yuxiang Zhou and Yulan He. Causal inference from text: Unveiling interactions between variables. In *Findings of the Association for Computational Linguistics: EMNLP 2023*, pages 10559–10571, 2023.